JOURNAL OF MATERIALS SCIENCE **38** (2003) 4581–4585

Preparation of nanosized particles of FeNi and FeCo alloy in solution

XIAOBO SU, HUAGUI ZHENG*, ZHIPING YANG, YONGCHUN ZHU, ANLIAN PAN
Department of Chemistry, University of Science and Technology of China, Hefei 230026, People's Republic of China

FeNi and FeCo alloys of different compositions are prepared at room temperature in solution by surface catalysis or high-pressure inducement. Their sizes and morphologies are analyzed with X-ray diffraction (XRD), high-resolution transmission electron microscope (HRTEM) and X-ray photoelectron spectroscopy (XPS). The phase transformations of these alloys are similar to the reported phase diagrams of FeNi and FeCo alloys. HRTEM image of $FeCo_4$ alloy shows the presence of rods. Their magnetic properties are studied. Surprisingly, the coercivity of $FeCo_4$ alloy reaches as high as 718 Oe.

1. Introduction

Fe_xNi_{1-x} alloys and Fe_xCo_{1-x} alloys exhibit a variety of structural, mechanical, and magnetic properties [1]. These unusual magnetic and physical properties include the condo effect [2] and invar phenomenon [3], which has led to diverse applications. For example, FeCo alloys, as traditional soft magnetic material, have the highest magnetic permeability and very good stability. Different applied fields have different requirement for *Hc* of the materials. How to increase *Hc* of alloys is an intriguing problem in material science, as permanent magnetic materials need to have high *Hc*. Nanosized particles of alloys exhibit properties, which drastically differ from the bulk [4]. As a possible solution of this problem, the preparation of superfine particles with homogeneous morphology and size is of great interest in the technological [5] and theoretical [6] fields. The properties and synthesis of nanoscale FeNi and FeCo alloys through physical method or solid state reactions have been studied, while superfine FeNi and FeCo alloys prepared in solution received much less attention [7]. Herein, we report the preparation of nanosized particles of FeNi and FeCo alloys by reduction of Fe (III), Co (II) and Ni (II) in alcohol-aqueous solution.

2. Experimental

The synthesis of FeNi and FeCo alloys was achieved by treating the solution of nickel (II) chloride, iron (III) chloride and cobalt (II) sulfate in ethanol with the mixture of hydrazine hydrate and sodium hydroxide. This reaction was completed at room temperature in alkalescent medium. X-ray diffraction patterns were collected on a Japan Rigaku $D/\max\ \gamma A$ diffractometer with Cu K_α radiation ($\lambda = 1.54178$ Å). HRTEM was performed on a JEOL 2010 high-resolution transmission electron microscope with an accelerating voltage of 200 kV. XPS spectra were obtained in ESCALAB MK II system with a base pressure of 1×10^{-9} mbar, in which Mg K_α radiation source ($h\gamma = 1253.6$ eV) was used. The M-H loops were measured by a model BHV-55 vibrating sample magnetometer at room temperature.

3. Results and discussion

The electromotive forces of Fe, Co and Ni for these reactions are as follows:

$$Fe(OH)_3 \xrightarrow{-0.56\,V} Fe(OH)_2 \xrightarrow{-0.877\,V} Fe$$

$$Co(OH)_3 \xrightarrow{0.17\,V} Co(OH)_2 \xrightarrow{-0.73\,V} Co$$

$$NiO \xrightarrow{0.49\,V} Ni(OH)_2 \xrightarrow{-0.69\,V} Ni$$

Ni (II) and Co(II) can be reduced by hydrazine directly in either water or ethanol, while surface catalysis or high-pressure induction [8] needs to be used for the reduction of Fe (III) and Fe (II) in the reaction mixture to avoid the kinetic difficulty.

3.1. Crystal structure types of FeNi alloys

When Fe (III) and Ni (II) are treated with hydrazine hydrate in alkalescent medium, $Fe(OH)_3$ are easily formed under the basic conditions. Ni(II) is readily reduced to Ni (0) particles for cooperation with hydrazine hydrate, which in turn reduce $Fe(OH)_3$ to Fe (0) particles as surface catalyst. When at.% of Ni is much higher than Fe (Fig. 1a and b), Fe atoms can easily enter the crystal lattice of Ni particles. The XRD pattern shows the characteristic peaks of γ-Ni. However, when at.% of Fe increases, it is difficult for Fe atoms to enter the crystal lattice of Ni particles. As a result, another phase α-Fe is formed, proven by its characteristic peaks in the XRD pattern (Fig. 1c). The phase transformation

*Corresponding author.

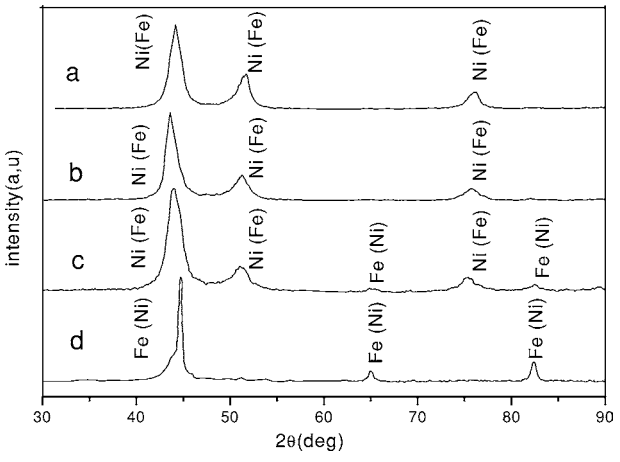

Figure 1 XRD patterns of FeNi alloys with various Ni contents. a = 80%, b = 75%, c = 60%, d = 20%.

from γ-Ni (Fe) to α-Fe (Ni) is clearly shown in XRD results (Fig. 1). When at.% of Fe is further increased to more than 80%, too much $Fe(OH)_3$ is formed to be reduced effectively so that most of $Fe(OH)_3$ aggregates to a more steady state. Therefore, high-pressure inducement is required to overcome the kinetic difficulty in reducing $Fe(OH)_3$. This was realized by heating the reaction mixture at 120°C in a high-pressure autoclave. Because the positions of characteristic peaks of alloys have been shifted from those of pure Ni and pure Fe in XRD patterns, the alloys are solid solutions rather than simple mixtures of two different phases of Fe and Ni. XPS also confirms that the prepared samples contain both Fe and Ni (Table I). The phase transformation with increasing at.% of Fe is similar to the phase diagram of FeNi alloys (Fig. 2) [9].

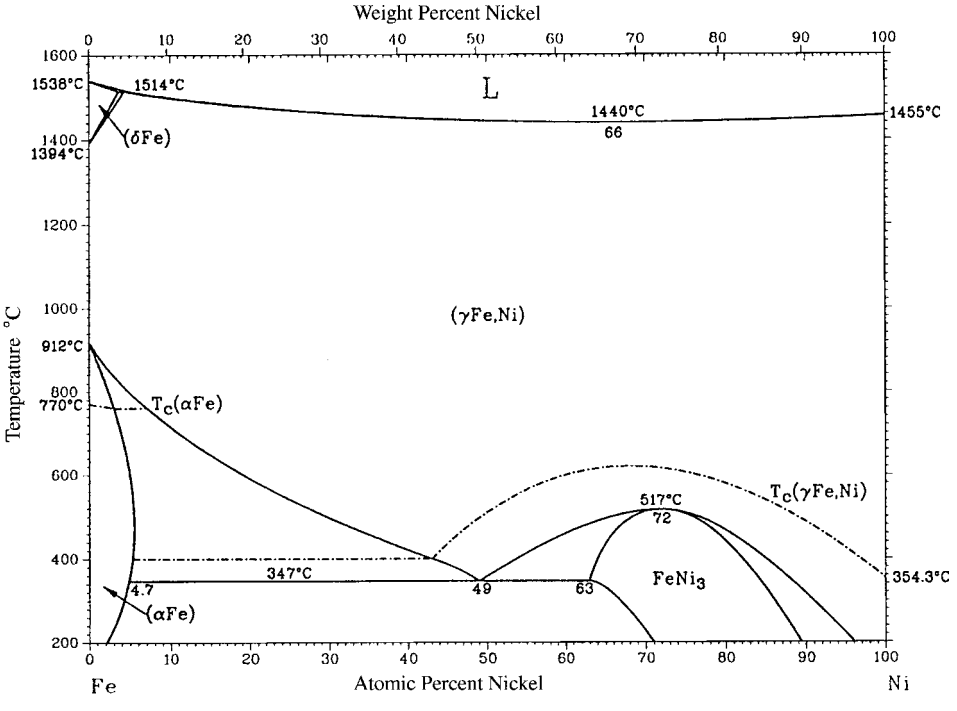

Figure 2 The phase diagram of FeNi alloys.

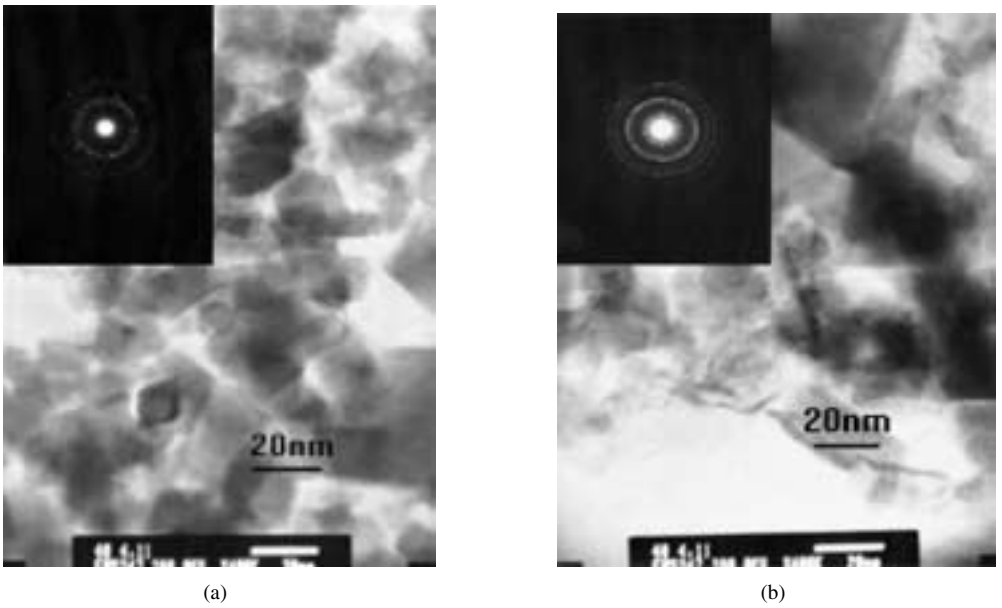

(a) (b)

Figure 3 (a) HRTEM image of Fe_4Ni alloy. (b) HRTEM image of $FeNi_4$ alloy.

TABLE I The quantification of XPS to the Fe_2Ni_3 alloy

Peak_ID	at%	Center	FWHM	Area	Normal	S.F	Stoic
01s	13.15	529.10	1.50	1511	2289	0.66	0.440
01s	31.85	530.65	1.50	3659	5544	0.66	1.065
01s	7.89	532.10	1.50	907	1374	0.66	0.264
Ni2P3	29.91	854.95	6.00	15623	5208	3.00	1.000
Fe2P3	17.20	705.90	3.40	5988	2994	2.00	0.575

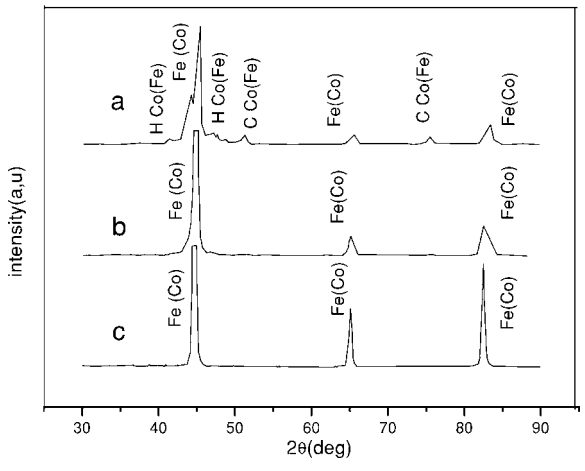

Figure 4 XRD patterns of FeCo alloys with various Co contents. $a = 80\%$, $b = 60\%$, $c = 20\%$.

3.2. Surface and microstructural characterization of FeNi alloys

3.2.1. XPS

Table I showed the quantitative results of O1s, Fe(2p) and Ni(2p) spectra decomposed from XPS spectra of Fe_2Ni_3 alloy. O1s peaks reveal the presence of three oxygen species, according to the signals from oxygen in the oxide (O^{2-}) at 529.10 eV, oxygen in hydroxyl group (OH^-) at 530.65 eV, and oxygen in water (H_2O) at 532.10 eV [10]. The relative atomic concentration of oxygen is fewer than that of pure Ni and Fe synthesized by the similar method, which shows that Fe_2Ni_3 alloy is more stable.

3.2.2. HRTEM

Fig. 3 gives the high-resolution transmission electron microscope images of Fe_4Ni (Fig. 3a) and $FeNi_4$ (Fig. 3b) alloys. Statistical analysis of Fig. 3a shows that the average size of the particles in Fe_4Ni alloy is smaller than 20 nm. Sharp rings can be seen in selected areas of the electron diffraction pattern. Analysis of Fig. 3b shows the average size of the particles is about 20–30 nm. Its electron diffraction rings are sharper and more diffraction spots indicate larger crystals. The increase of the particle size to 20–30 nm is probably due to surface catalysis by Ni. Therefore, the size and morphology of the alloys can be changed by adjusting the proportion of Fe and Ni.

3.3. Crystal structure types of FeCo alloys

XRD patterns of samples with different proportions of Fe and Co are shown in Fig. 4 When at.% of Co equals to 80%, there are three phases in the mixture: hexagonal Co, cubic Co and α-Fe. When at.% of Co is less than 60%, Co atoms enter the crystal lattice of Fe particles. Because of electromotive forces of Co(II) and Ni(II) given above, synthesis of Co is slower than that of Ni, making it less capable of surface catalyzing the reduction of Fe (III), Fe (III) cannot be reduced quickly and

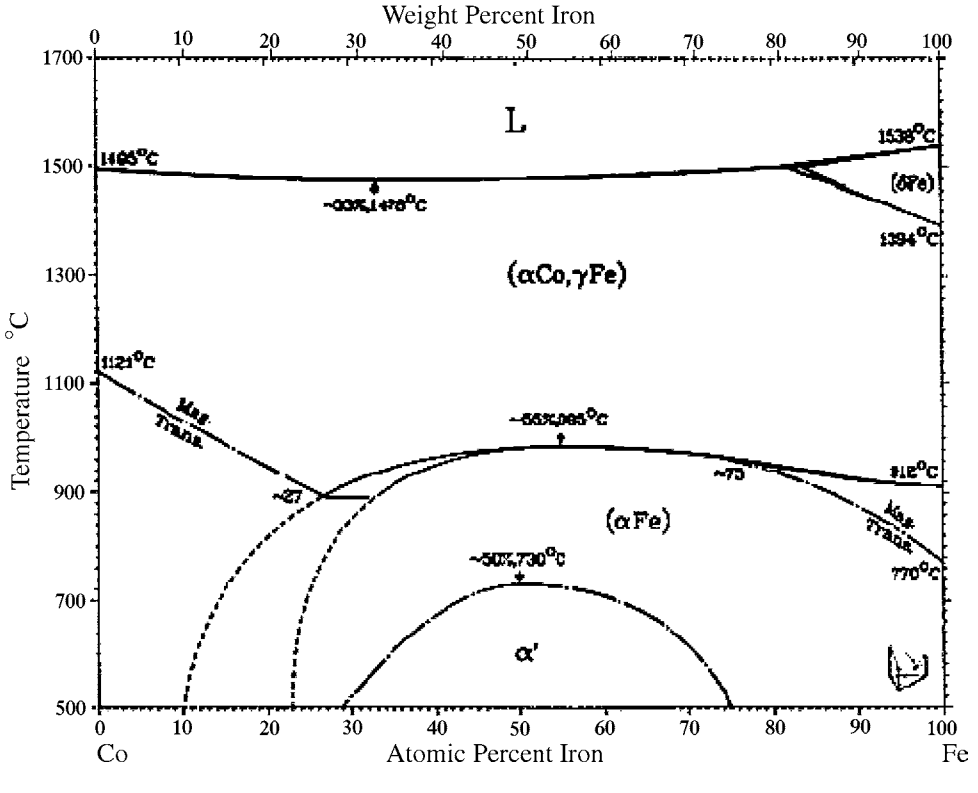

Figure 5 The phase diagram of FeCo alloy.

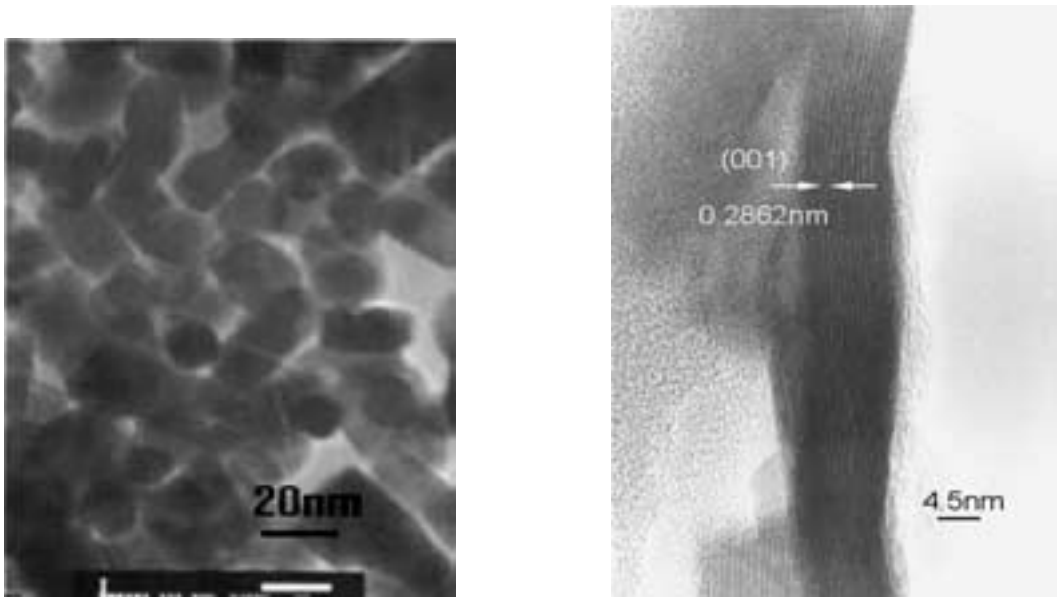

(a) (b)

Figure 6 (a) HRTEM image of Fe_4Co alloy. (b) Magnified HRTEM image of $FeCo_4$ alloy.

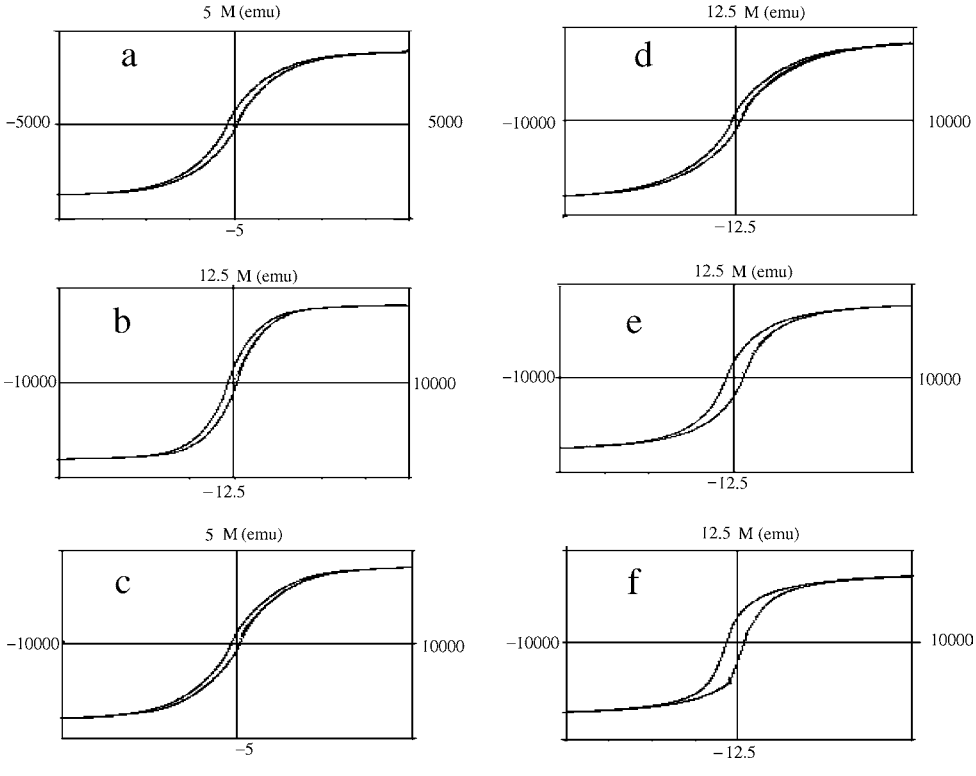

Figure 7 M-H loops of FeNi and FeCo alloy with different contents 80%Ni-20%Fe (a), 60%Ni-40%Fe (b), 20%Ni-80%Fe (c), 80%Fe-20%Co (d), 40%Fe-60%Co (e), 20%Fe-80%Co (f).

α-Fe (Co) phase appears at lower at.% of Fe in FeCo alloys than in FeNi alloys. The phase transformation with increasing at.% of Fe is similar to the phase diagram of FeCo alloys [11] (Fig. 5).

3.4. Surface and microstructural characterization of FeCo alloys

3.4.1. XPS

XPS spectra of Fe_4Co alloys are similar to those of FeNi alloys as shown in Table II. It does not contain the characteristic peak of water. The greater percentage of oxygen in the composition of the samples' surface shows that FeCo alloys are less stable than FeNi towards oxidation by air.

3.4.2. HRTEM

Fig. 6a shows the HRTEM image of Fe_4Co alloy. The average size of particles is found to be about 20 nm by statistical analysis. Around 5% of the $FeCo_4$ alloy consists of rods. Fig. 6b gives the enlarged image of a rod,

TABLE II Quantification of XPS to Fe_4Co alloy

Peak_ID	at%	Center	FWHM	Area	Normal	S.F	Stoic
01s	23.69	528.90	1.95	5531	8380	0.66	1.000
01s	55.39	531.30	2.10	12932	19594	0.66	2.338
Co2p3	8.68	780.95	10.35	7680	3072	2.50	0.367
Fe2p3	12.24	709.50	4.20	8659	4329	2.00	0.517

from which the clear lattice fringes can be observed. The lattice spacing is 2.862 Å, corresponding to (001) plane of α-Fe (Co).

3.5. Magnetic properties

Fig. 7 shows the magnetization curves of FeCo and FeNi alloys with selected compositions at room temperature. $FeNi_4$ alloy has a coercivity of 141 Oe (Fig. 7a). When at.% of Fe increases, the magnetization increases. The coercivity of Fe_4Ni reaches 244 Oe. Similar change is also found in FeCo alloys but more dramatic with the increase in at.% of Co. The coercivity jumps from 244 Oe for Fe_4Co to 718 Oe for $FeCo_4$. When the shape anisotropy of magnetic grain was very high, high coercivity can be obtained [12]. Higher coercivity obtained for $FeCo_4$ alloy is probably due to the presence of anisotropic rods as found in HRTEM image of $FeCo_4$ alloy.

4. Conclusion

Nanoparticles of FeNi and FeCo alloys are successfully prepared in alcohol-aqueous system by using surface catalysis and high-pressure inducement. The phase transformations of these alloys are similar to the reported phase diagrams of FeNi and FeCo alloys. The presence of rods in $FeCo_4$ alloy may be responsible for its unusual high coercivity of 718 Oe. Currently, efforts are underway to increase the yield of rods and to study other relative properties of these alloys.

References

1. F. SCHEDIN, L. HWEITT, P. MORRAL, V. N. PETROV and G. THORNTON, *J. Magn. Magn. Mater.* **198** (1999) 555.
2. J. KONDO, F. SEITZ, D. TURNBULL and H. EHRENREICH, *Solid State Phys.* (1969) 23.
3. E. F. WASSERMANN, *Adv. Solid State Phys.* **27** (1987) 85.
4. R. SIEGEL, *Nanostr. Mater.* **3** (1993) 1.
5. G. BATE, *J. Magn. Magn. Mater.* **100** (1992) 413.
6. D. D. AWSCHALOM, D. P. DIVINCENZO and J. F. SMYTH, *Science* (1992) 258.
7. R. BOLSONI, V. DRAGO and E. LIMA, *Mater. Sci. Forum.* **403** (2002) 51.
8. H. G. ZHENG, J. H. ZENG, H. M. YU, Y. J. ZHANG, J. H. LIANG and Y. T. QIAN, *J. Ustc.* **6** (1999) 29.
9. L. J. SWARTZENDRUBER, V. P. ITKIN and C. B. ALCOCK, "Binary Alloy Phase Diagrams" (1991).
10. F. M. JOHN, *et al.* "Handbook of X-ray Photoelectron Spectroscopy" (Physical Electronics Inc. Minnesota, 1992).
11. T. NISHIZAWA and K. ISHIDA, "Bull. Alloy Phase Diagrams" (1984).
12. D. H. QIN, L. CAO, Q. Y. SUN, Y. HUANG and H. L. LI, *Chem. Phys. Lett.* **358** (2002) 484.

Received 29 July 2002
and accepted 7 July 2003